

Development of a genetic algorithm for maximizing the light induced heat generation of nano-plasmonic antennas

Lars Nolden^{1*}, Dr. Sven Askes², Dr.ir. Boukje de Gooijer²

¹ University of Twente, Faculty of Engineering Technology, Drienerlolaan 5, 7522 NB, Enschede, The Netherlands

²Vrije Universiteit Amsterdam, Faculty of Science, De Boelelaan 1081 , W&N building, 1081 HV, Amsterdam, The Netherlands

*l.nolden-1@student.utwente.nl

ABSTRACT: Efficient light to heat conversion in nano-plasmonic antennas is crucial for possible cancer treatment technologies and to further the understanding of plasmonic effects. Metallic nano-particles when exposed to optical fields can couple with electron excitations leading to plasmons. Which drastically change the particles light absorption properties. This effect is highly dependent on the nano-antennas material, shape and size of the particle. Furthermore, formal methods relating the particles properties to its light absorption are largely absent, with the exception for spherical particles that are well described by Mie-theory. Therefore the plasmonic effects and possible interactions between multiple nano-particles of non-spherical shape are hard to determine analytically. Such that for novel shapes a simulation is required to determine their absorption levels. This research shows the utilisation of a genetic algorithm to generate novel nano-plasmonic antenna designs that maximize the incident light to heat conversion. While taking into account the current manufacturing constraints for nanoparticles. The results show a convergence of the genetic algorithm towards a specific antenna design that favors smaller particles and close contact (less than 10nm) between the domains, aligning with the theory of hybridized plasmon modes.

Key words: Nanophotonics, Plasmonics, Generative Design, Genetic Algorithm, Hybridized Plasmon Modes

1 INTRODUCTION

Metallic materials exhibit the ability to couple optical fields with electron excitations. The coupling originates from collective excitations by the incident electro-magnetic light wave. These collective excitations are termed plasmons, giving rise to strong optical absorption levels for these particles.

Multiple types of collective excitation patterns exist. Surface Plasmon Polaritons (SPPs) requires momentum matching through techniques like grating coupling or prism coupling (Kretschmann configuration) to introduce collective oscillations that propagate along the interface of a the film and its dielectric. Localized surface plasmonic resonances (LSPRs) require at least one dimension the nano-particle to be much shorter than the wavelength of the incident light $L \ll \lambda$. Such that a nearly constant phase is induced by the incident light across the short side of the particle. The changing phase over time due to the wave nature of the incident light will introduce oscillations. A metallic nano-particle made of gold, silver, copper or aluminium exhibits plasmon resonances at

certain wavelengths, which depend on the material properties (dielectric function), shape and size of the nano-particle.¹ Particles that are designed to feature a specific resonance frequency are defined as nano-antennas.

Nano-antennas can concentrate and manipulate incident light at the nanoscale, enabling a wide set of applications from enhanced spectroscopy to potential cancer treatment technologies.

Efficient light-to-heat conversion is crucial for several applications. Such as photo-thermal therapy where targeted heat generation can be used to destroy cancer cells.² Photo-thermal catalysis also greatly benefits from improved light absorption and heat conversion, as these enhancements can boost catalytic reactions. This effect can be used in a multitude of chemical processes, including the thermal degradation of organic pollutants in water.³ Therefore, by optimizing light-to-heat conversion we increase the viability of these technologies.

The possible design space for a nano-antennas is very large and intractable in size for a human designer to arrive at a satisfying design solution within a realistic

time frame due to the high number of dependencies on the resonance frequency of a nano-antenna and the complex nature of possible antenna shapes that influence the resonance intensity. This research will investigate an alternative, genetic algorithm based approach to overcome this challenge.

Generative design aids in exploring such a large design parameter space. By attempting to find a globally optimal or near-optimal solution in the design parameter space through several heuristics.

The genetic algorithm is an iterative optimization process inspired by natural selection. Each candidate solution to the objective has a unique set of properties encoded as digital chromosomes.

The fitness function represents the objective to be optimized for and feeds back a fitness score to evaluate each candidate. Such as the calculated signal strength in an antenna or the ultimate tensile strength of a material composite. Fitness functions can use a multitude of methods to obtain the fitness score. Such as analytical analysis or finite element method modelling. They represent the only connection between the domain problem and the genetic algorithm.

For each generation of the optimization process, the fittest candidates are selected (selection process) and recombined with each other. Where traits of the candidates are combined to form a new generation of candidates (crossover process). Furthermore, some genetic variance via mutations is introduced (mutation process). This will enable the process to explore the solution space adequately and prevent converging around local maxima. The termination function that will stop the iterative process can be defined as a certain number of generations, a certain achieved fitness score or as the convergence of candidate solutions.

Existing research that leverages genetic algorithm in order to optimize the behaviour of plasmonic nano-antennas relies on Rigorous Coupled Waves Analysis (RCWA)⁴ or Finite Difference Time Domain (FDTD)⁵ simulations to assess the fitness of an individual. This research shows how to utilize a Finite Element Method (FEM) to arrive at a nano-antenna design optimized for the conversion of incident light to heat.

The simulation setup and the tuning of the genetic algorithms parameters are described. We introduce and contrast methods for determining these parameters to ensure the algorithm's convergence. A series

of mesh sensitivity evaluations is conducted in order to determine a sufficient mesh resolution. Complemented by a posterior model accuracy test. Moreover, the results from computations that created over 2900 novel antenna designs are evaluated on their light-to-heat conversion performance. The convergence of the algorithm to a certain shape is illustrated. More detailed analysis on the best and worst performing antenna design is performed with electric field intensity and energy absorption plots. Further a physics based interpretation of the convergent antenna properties is given.

2 METHODOLOGY

2.1 Manufacturing Constraints

Common nano-scale manufacturing processes are Focused Ion Beam (FIB) milling and E-beam lithography. FIB is an imperfect subtractive milling process via ion beams and less precise than E-beam lithography. E-beam lithography is the more precise technology. Which utilises an electron beam to draw patterns on an electron-sensitive resist. The resolution of E-beam lithography is limited mainly by the forward scattering of electrons in the resist. Where incoming electrons scatter laterally upon interacting with the resist and therefore expose areas wider than intended by the beam width.⁶ Currently the highest resolution achievable with E-beam lithography is 2nm isolated feature size and 5nm half-pitch size.⁷ More common are resolutions of gap widths ranging from 4nm⁽⁸⁾ to 10nm⁽⁹⁾ and possible radii between 8nm to 15nm⁽¹⁰⁾. Therefore, these manufacturing constraints must be taken into account for the simulation of the particle if the goal is to generate real-world reproducible solutions.

Each candidate solution is represented by a chromosome string of 121 binary values, restricting the possible solution space. The binary representation allows easy manipulation and merging of chromosomes by the genetic algorithm. Furthermore this representation creates a human relatable connection between the chromosome string and the resulting antenna shape. The string is converted into a map of 11×11 pixels that cover the substrate size of 500nm \times 500nm. Therefore each of these pixel is 45.4nm \times 45.4nm in size. Padding of 20nm is added to avoid shapes that

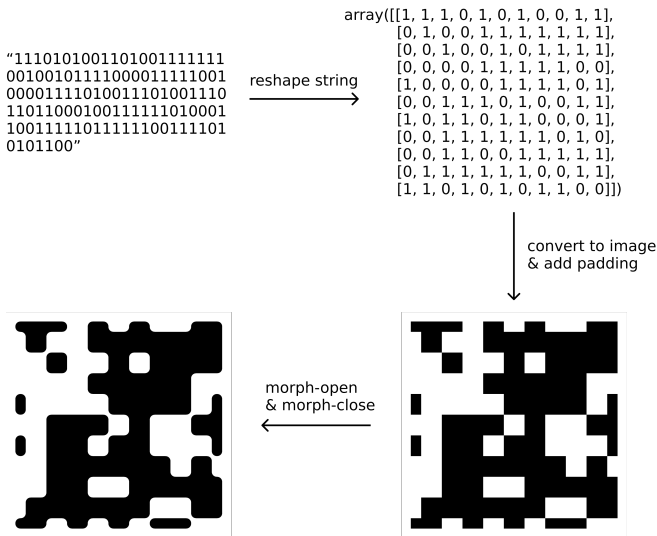


Fig. 1: Process of converting the chromosome representation to a shape

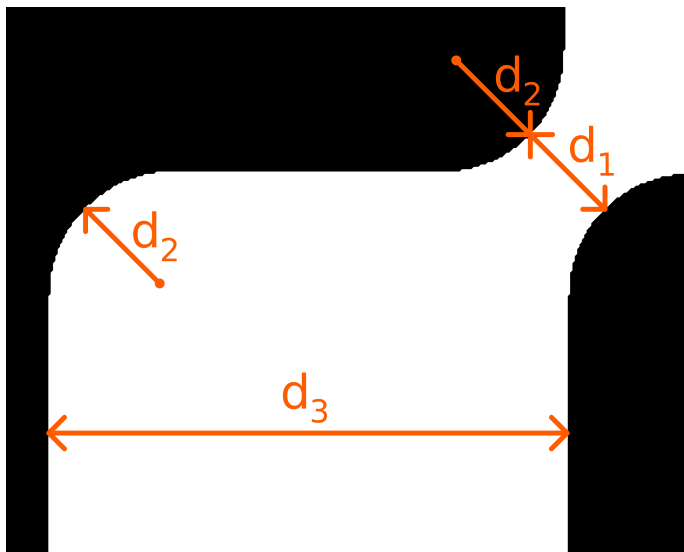


Fig. 2: Enlarged section displaying the dimensions
 $d_1 = 9.4\text{nm}$, $d_2 = 9.1\text{nm}$ and $d_3 = 46\text{nm}$

touch the substrate boundaries leading to undefined behaviour. Two morphological transformation kernels are applied to the image in order to represent the manufacturing constraints of the rounded corners. First an opening operator and then a closing operator are applied by an elliptical kernel on the images pixels. The kernel size (s_{kernel}) depends on the desired fillet radius (r_{fillet}) and image resolution (ppn) (Equation 1). The OpenCV (Open Computer Vision) Python library is used to apply the operations on the image.¹¹ Mentioned instructions can be found in Appendix A.

$$s_{kernel} = 2 r_{fillet} ppn \quad (1)$$

Where ppn is the pixel per nanometer.

The resulting smallest dimensions of the antenna are radii of 9.1nm and diagonal gap distances of 9.4nm as shown in Figure 2 and therefore align with the current resolution limits of E-beam lithography.

This morphed image is converted into two distinct section wise contour files. An inner and outer contour file, where the inner contour file is utilised in COMSOL to subtract holes from the outlines generated by the outer contour file. Each contour file is processed by an interpolation function to generate a surface, which is then extruded to a height of 40 nm .

2.2 Simulation Setup

The antenna is placed on a substrate with a refractive index of 1.5 matching the behaviour of glass material at around 532nm . In contrast, the surrounding air volume is modelled with a refractive index of 1. The incident light has a wavelength of 532 nm and is tangential to the substrate surface, as shown in Figure 3. Ag (Silver)¹² material is selected for the the antennas material composition.

The substrate is square shaped, spanning a side length of 750nm . Notably, the incident light source is at a distance of 360 nm to the surface of the antenna. More than half the incident lights wave length. The vertical boundary surfaces of the simulation feature periodic conditions to simulate the behaviour of a nano-antenna array.

2.3 Software

The COMSOL Multiphysics FEM software is used for the simulations, controlled programmatically via the API by the genetic algorithm. For the genetic algorithm's implementation, the PyGAD¹³ Python library is used.

2.4 Compute

The genetic algorithm is run on an AMD Epyc 7212 with 16 cores and 128 GB of system memory. Each simulation takes on average 9 minutes and 31 seconds to complete with four simulations running in parallel. A total of 2908 simulations were computed.

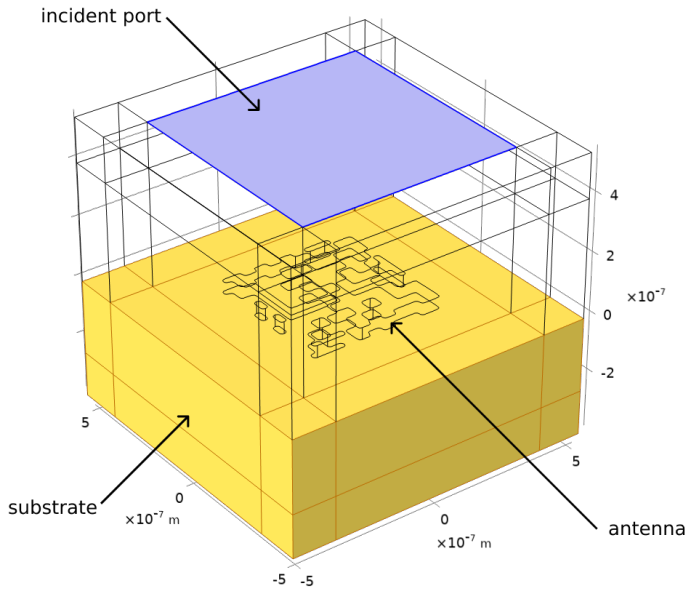


Fig. 3: Simulation setup showing the incident light port (highlighted blue), the substrate (highlighted yellow) and the outlines of an example antenna shape.

2.5 Mesh Sensitivity

The optimal mesh resolution for the air and nano-antenna domains are determined. Computational cost reflected in required computation time and simulation accuracy require balancing in order to achieve satisfactory simulation accuracy that drives convergence of the genetic algorithm to a design that performs well when reproduced and further, increasing the number of possible solutions generated over the run-time of the generative design process to explore the solution space as much as possible.

For this purpose a randomly chosen antenna design with medium complexity and element count is benchmarked with various mesh size settings in Table 1. The different mesh sizes are chosen from the predefined COMSOL meshing presets. From the benchmark results it was concluded that a *Fine* meshing resolution is applied. Such that a decreased simulation run time is traded with an increased error. While an error of 19% seems significant, the primary objective is not to achieve high individual candidate accuracy. But rather sufficient precision that leads the genetic algorithm to a convergence of antenna features

that enhance performance in real world reproductions. Furthermore, the top performing solutions are simulated again at a higher mesh resolution manually for verification purposes of the results.

2.6 Figure of Merit

The genetic algorithm optimizes for light induced heat generation through plasmonic effects only indirectly. Total light absorption is used as a proxy for light induced heat generation in order to reduce model complexity.

$$f(i) = \iiint_{V_{\text{antenna}}} Q_h dV \frac{1}{I_0 w^2} \quad (2)$$

The fitness of individual i is given by $f(i)$ (Equation 2). Where the total power dissipation $Q_h [\text{W m}^{-3}]$ is integrated over the volume of the nano-antenna. And divided by the product of the incident field intensity $I_0 [\text{W m}^{-2}]$ and the light port surface area w^2 . The result is a dimensionless number that indicates how much of the incoming lights power is absorbed by the particle. This figure of merit aligns with the general interest of understanding the influence of a nano-plasmonic antennas shape and cross antenna interactions on plasmonic heating and more generally the interaction between light and matter at the nano-scale.

The maximal achievable fitness is limited by the ratio of the incident light port surface area and the maximum surface area of the the nano-antenna. In the given simulation setup the nano-antenna surface area can be at most 37% of the incident light port surface area. Therefore only at most are 37% of the incident light absorbed by the nano-antenna. Although, this is not considering any plasmonic enhancement effects which could increase this theoretical limit. This has to be taken into account when analyzing the results of this antenna performance. It is not relevant for the convergence of the genetic algorithm as the best performing result is still far from this theoretical maximum.

2.7 Genetic Algorithm Parameters

The behaviour of a genetic algorithm can vary greatly due to the parameters configured. Available parameters include, but are not limited to the number of solutions per generation, the number of parents mating

Mesh	Time Factor	Error %	Domain Elements	Boundary Elements	Edge Elements
Coarse	1	57	59 079	14 470	2043
Normal	1.01	74	59 281	14 472	2044
Fine	1.37	19	91 343	18 129	2370
Finer	2.77	4	257 541	34 990	3335
Extra Fine	11.68	0	993 533	88 633	5384

Table 1: Mesh sensitivity benchmark comparing the relative time factor and relative error percentage are shown. The fastest simulation (*Coarse*) is taken as the base value for the time factor. And the most accurate simulation *Extra fine* is taken as the Error percentage base value.

and the mutation probability. A heuristic fitness function is derived in order to find a suitable set of parameters. This heuristic function allows us to test a very large amount of possible parameter sets due to its very low computational effort. A full genetic algorithm run with 40 solutions per population and 200 generations can be achieved in less than 30s when using the heuristic fitness function instead of the actual fitness function that utilises the FEM simulation. The goal of the heuristic fitness function is to be low in computational effort while mirroring as much of the real fitness functions behaviour as possible.

Two distinct methodologies are employed to conceptualize the heuristic fitness function. In the first approach, multiple Gaussian kernels are positioned on the nano-antenna grid, representing an arbitrary desired shape. Such that every pixel within the grid correlates to a fitness score based on the proximity to the desired shape, as shown in Figure 4. Then, the candidates fitness is computed as the sum of all the pixels individual fitness values that were placed by the algorithm. Therefore a higher fitness score would indicate a higher resemblance to the desired shape. With a fitness reward that scales non-linearly with the proximity to the intended shape. The resulting parameters of this approach did not yield any significant fitness increase with prolonged simulation run time and are therefore deemed to be unsuitable (Figure 5).

The second approach features a simple summation of the binary chromosome representation where the higher sum leads to a higher fitness. This approach led to a different set of parameters that increased the fitness of the solution with simulation run time (Figure 5). Final parameters can be found in Appendix B.

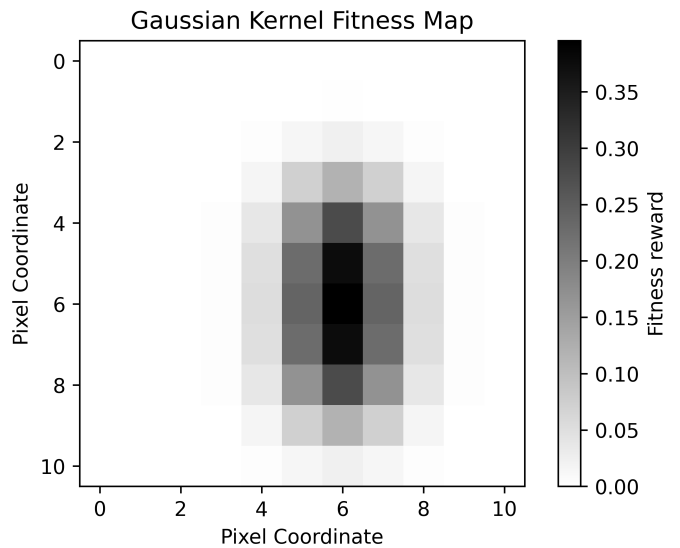


Fig. 4: The fitness map displays the fitness score for each pixel based on its specific coordinate. The darkest points correspond to the arbitrarily selected shape. Pixels surrounding this chosen shape, as determined by the algorithm, receive decreasing rewards as their distance from the target shape increases.

3 RESULTS

3.1 Detailed Mesh Investigations

As highlighted in subsection 2.5 the simulations are run on a *fine* mesh preset to balance accuracy and compute time. We compare impact of this choice on multiple simulation results and verify if the chosen mesh resolution is sufficient for the genetic algorithm to converge towards a good solution. The top 20 solutions with the highest fitness score and 20 other randomly sampled solutions are re-meshed in the *finer* meshing preset yielding a higher accuracy closer to the real world performance. Computed results indicate a mean difference in fitness of

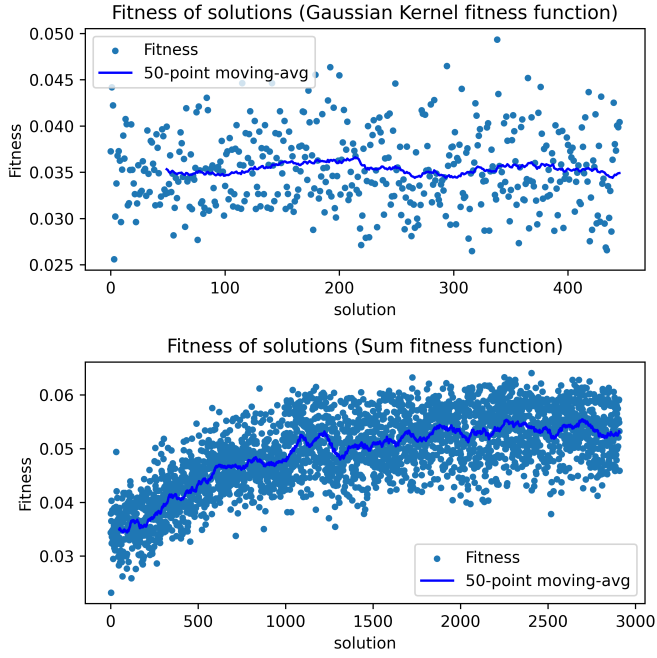


Fig. 5: The two heuristic sets applied to the real fitness function. The moving average of the solutions fitness indicates stagnant behaviour for the gaussian kernel fitness function approach. And an increase in fitness with each solution for the sum fitness function approach.

$\bar{x}_{fitness} = 0.00998 \approx 1\%$. Therefore on average the the results of the finer mesh resolution are close to that of the *fine* mesh resolution. The high coefficient of variation $CV_{fitness} = 0.5924$ in respect to the fitness error shows that the simulation error varies greatly over the sample data set. Although this does not necessarily indicate an inadequate meshing resolution but significant simulation inaccuracies. Interestingly Figure 6 displays that a higher error is generally related to a higher computed fitness at lower (original) mesh resolution. Overall the comparison displays that the *fine* mesh resolution is an adequate balance between accuracy and computation time.

3.2 Best Solution

The best performing shape, displayed in (Figure 7) has a light to heat conversion ration of 6.4%. The shape features high resemblance to the pixels associated with high fitness in Figure 7.

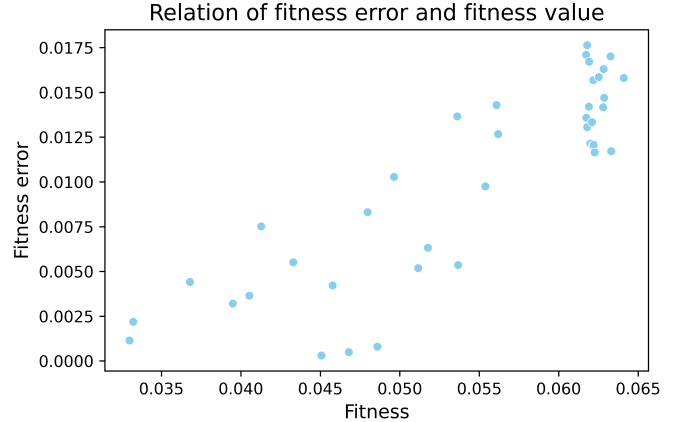


Fig. 6: Scatter plot showing a relation between the fitness error and the fitness computed by the genetic algorithm. The error is the absolute value between the fitness computed with *finer* and *finer* mesh resolution. It is notable that the error increases with the fitness value. The fitness difference tends to be larger more often and not evenly distributed. Reflected in the computed Coefficient of variation of $CV_{fitness} = 0.5924$.

3.3 Shape Convergence

The generative design process converged to a certain shape. As shown in Figure 7, there are certain pixels for which the normalized fitness is higher than others. This indicates a relationship of high fitness with a specific pixel placement has been discerned by the algorithm. A large count of pixels with high normalized fitness is therefore also present in the best performing solution.

3.4 Frequency Sweep

A frequency sweep is performed in order to verify a peak response at 532 nm of the top performing candidate. The results of the frequency sweep in Figure 8 show that 532nm is indeed a resonance wavelength. A wide resonance response from about 390nm and 540nm is identified.

3.5 Antenna Design and Performance

It is found that the surface area of the antenna and the candidates fitness has a negative correlation coefficient of $\rho_{area,fitness} = -0.598$, which indicates that antennas with a smaller total surface area generally perform better. Further the correlation between

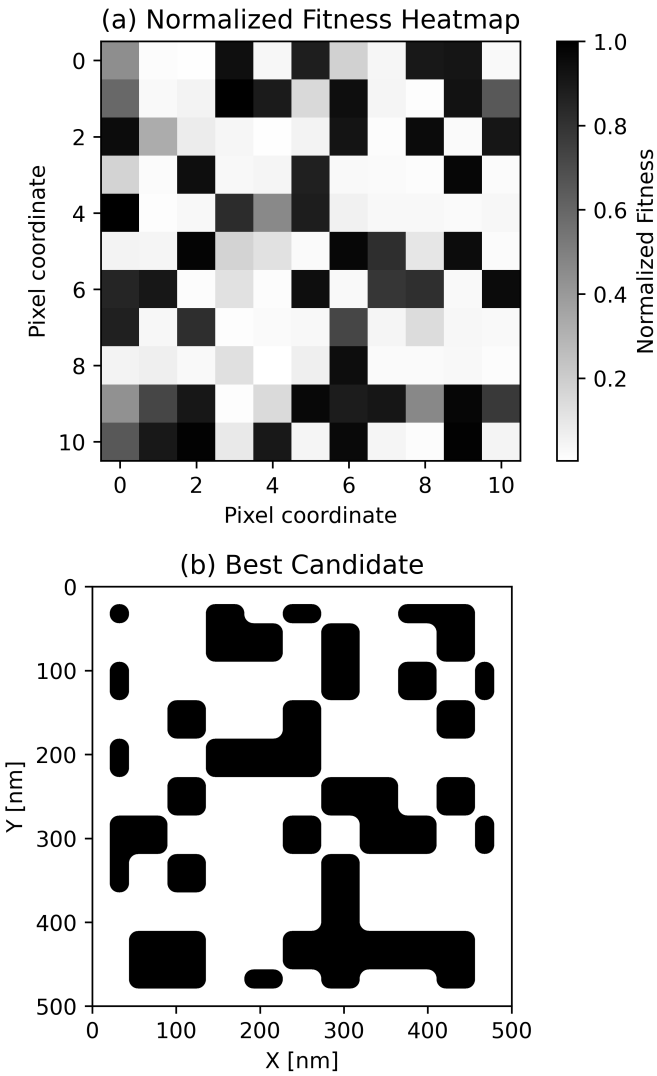


Fig. 7: (a) The fitness of each pixel normalized across all solutions. Displaying convergence to certain shapes favoring pixels associated with high solution fitness. (b) Shape of the best performing solution (black pixels correspond to material, white pixels show substrate) with a light to heat conversion ratio of 6.4%. Created in generation 70 of 85 total generations.

the number of domains (antenna islands) and the candidates fitness of $\rho_{nDomains,fitness} = 0.544$ indicates that more domains generally lead to a better performance.

3.6 Comparing Candidates

In Figure 9 the best and worst performing candidates are compared visually with electric field intensity plots and power dissipation density plots. The

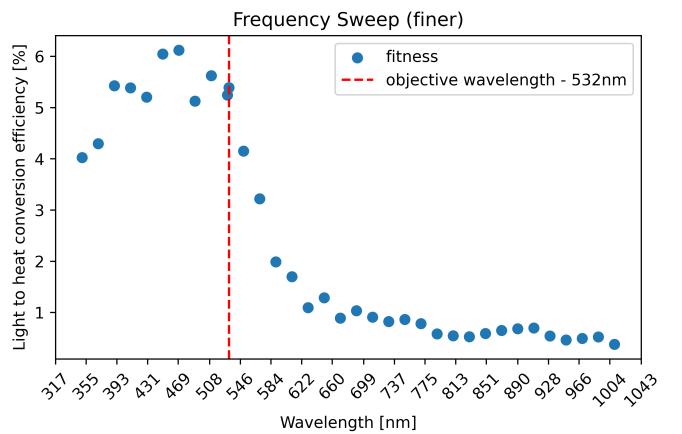


Fig. 8: Frequency Sweep with *finer* mesh resolution. The red line indicates the optimization wavelength of 532nm. A peak excitation between 390nm and 540nm is visible.

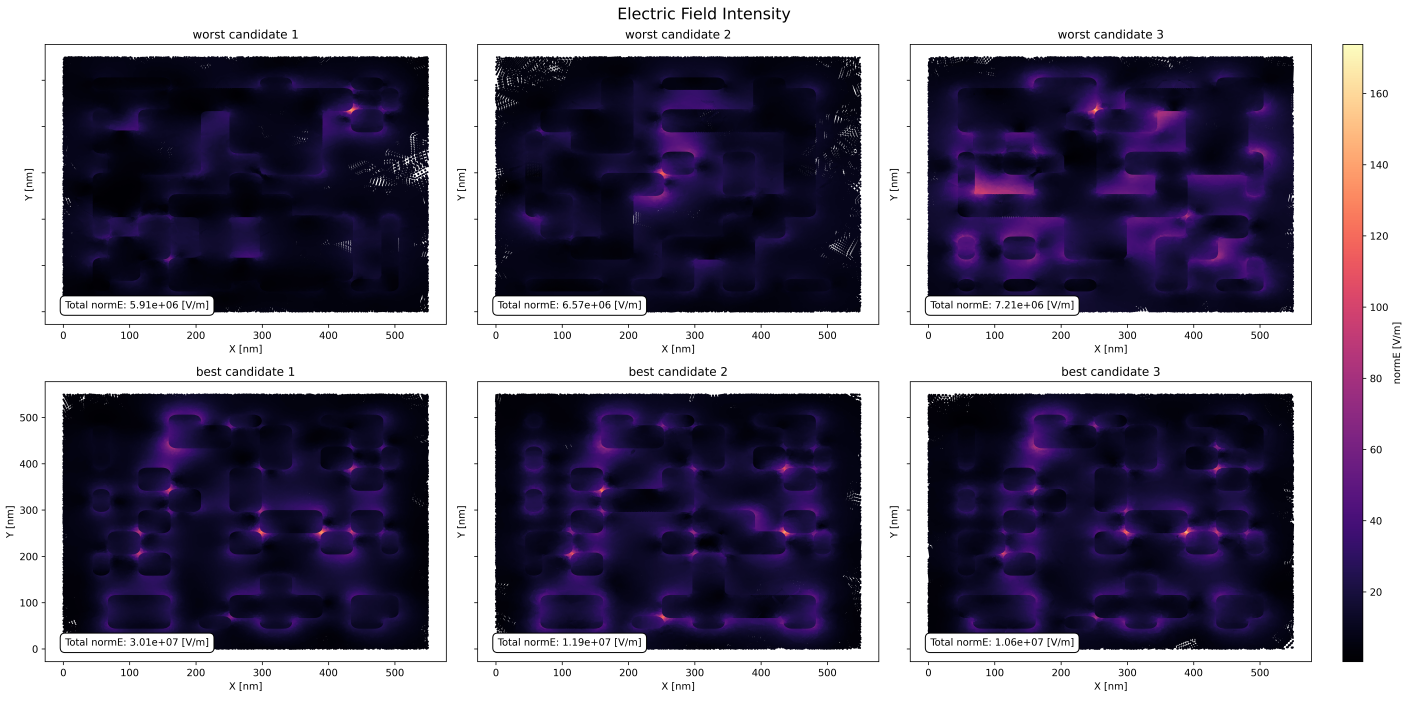
brightest spots show the electric field and power dissipation hot-spots. The theoretical correlation of a high electric field intensity leading to a high amount of dissipated power in the particle is clearly visible when comparing the bright spots of (a) and (b). The total electric field intensity in (a) is significantly larger for the best performing candidates compared to the worst performing candidates. Which can also be confirmed visually. This observation translates to the power dissipation density in (b). Therefore more power is absorbed by the best particles and converted to heat. Most of the hot-spots occur in between the diagonal gaps (d_1 in Figure 2) between particles with a gap distance of 9.1nm. It can be concluded that the algorithm successfully maximized the main objective of increasing the power absorption of the nano-antenna.

4 DISCUSSION

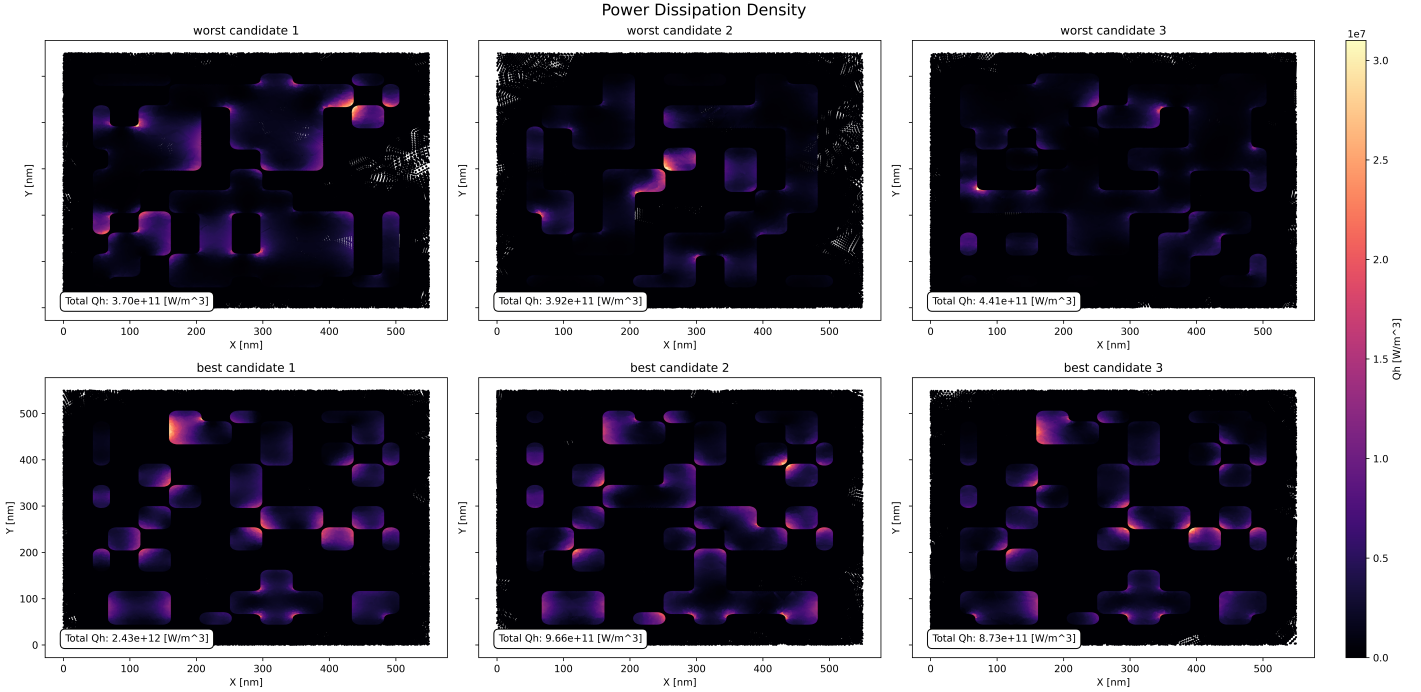
4.1 Physical Phenomena

The strong electric field enhancements between the antenna gaps could be attributed to the interaction similar to that between nano-particle dimers. This phenomenon is well-understood and has been extensively researched in existing literature. Significant electric field enhancement are shown to emerge when two Au (gold) or Ag (silver) nano-particles are in close proximity.¹⁴

The plasmon hybridization theory provides a comprehen-



(a) Electric field intensity at half the antenna height. The total intensity of the best design is about 1.7 times higher than that of the worst design. Most hot-spots of high electric field intensity originate between gaps of diagonal elements. To note is the hot-spot in the third worst candidate on the inside of a 90 degree antenna bend.



(b) The power dissipated at half the height of the best performing and worst performing produced antenna designs seems to be related to the electric field intensity visible Figure 9a. As the spots of high power dissipation overlap with that of high electric field intensity.

Fig. 9: Combined figure of Electric field intensity and Power dissipation density plots of the three best and worst performing produced antenna designs.

hensive framework to understand this interaction.¹⁵ This method describes the plasmons of a complex nano-particle as the hybridization of the individual nano-particles plasmons. When these particles approach each other, their plasmons can interact and form new collective modes. The “bonding” mode, which is a lower energy mode, arises when the charges of the two nano-particles oscillate in phase. This mode is often responsible for the strong field enhancements observed in nano-gaps. On the other hand, the “antibonding” mode is a higher energy mode where the charges of the two nano-particles oscillate out of phase. Which typically does not lead to a strong field enhancement.¹⁶

The proximity and geometry of the nano-particles are the determining factors in the field enhancement intensity. As the gap between the nano-particles decreases, especially in the sub-10 nm regime, quantum effects can also come into effect,¹⁷ leading to other behaviors that may deviate from predictions based solely on electrodynamics. Such effects can include electron tunneling across the gap, further modifying the plasmonic response.

4.2 Improvements

The quality of the results is restricted by the total computation time. An increase in total computation time or a reduction of required computation time for a single simulation would increase the result quality. The total computation time for a single candidate varies greatly with the complexity of the antenna shape, of which on average of 87% are spent running the FEM solver. Therefore a speed up of the FEM solver would yield the biggest benefits. Further, the required computation time scales with the number of nodes in the geometries mesh. A more compact and reduced version of the simulation geometry would reduce the number of nodes. The total simulation volume of surrounding air and dielectric could be reduced to a minimum. By running a series of simulation accuracy regression tests with ever decreasing total simulation volume.

Further improvements could be achieved by reducing the number of solutions required until convergence is reached. This could be achieved by determining more optimal parameters for the genetic algorithm via a more sophisticated heuristic fitness function. Such function would be required to mirror the performance

results of the true antenna simulation as best as possible. While requiring significantly less computation time. Possibly a reduced simulation setup could function as a heuristic fitness function to explore the parameters.

5 CONCLUSIONS

The development of a genetic algorithm that utilises a finite-element-method simulation to optimize pixelated nano-antennas for power absorption performance is shown. Impressively does the algorithm show successful convergence towards a specific structure as highlighted in Figure 7.

While the frequency sweep indicates some fluctuations in the fitness values around similar wavelengths, indicating the need for higher meshing resolution. A strong correlation between the antenna shape and fitness value can be highlighted. This strong correlation underscores the algorithms ability to capture the relationship between the nano-antenna design and absorption performance.

Further, the convergence shows a generally higher absorbed power for nano-antennas with many domains and high numbers of diagonal gaps. In alignment with plasmon hybridization theory.

Although it is unclear how the found solutions perform in a physical experiment, this implementation can be a further improved and hopefully contribute to the fields of photo-thermal catalysis and heating.

ACKNOWLEDGEMENTS

This work would not have been possible without my supervisors Dr. Sven Askes and Dr. Boukje Gooijer.

REFERENCES

- (1) Jain, P. K.; Lee, K. S.; El-Sayed, I. H.; El-Sayed, M. A. *Journal of Physical Chemistry B* **2006**, *110*, 7238–7248.
- (2) Huang, X.; El-Sayed, I. H.; Qian, W.; El-Sayed, M. A. *Journal of the American Chemical Society* **2006**, *128*, 2115–2120.
- (3) Wei, H.; Loeb, S. K.; Halas, N. J.; Kim, J.-H. *Proceedings of the National Academy of Sciences* **2020**, *117*, 15473–15481.

- (4) Mayer, A.; Bi, H.; Griesse-Nascimento, S.; Hackens, B.; Loicq, J.; Mazur, E.; Deparis, O.; Lobet, M. *Opt. Express* **2022**, *30*, 1167–1181.
- (5) Li, D.; Zhou, H.; Hui, X.; He, X.; Mu, X. *Analytical Chemistry* **2021**, *93*, PMID: 34170680, 9437–9444.
- (6) Broers, A. N.; Hoole, A. C. F.; Ryan, J. M. *Microelectronic Engineering* **1996**, *32*, 131–142.
- (7) Manfrinato, V. R.; Zhang, L.; Su, D.; Duan, H.; Hobbs, R. G.; Stach, E. A.; Berggren, K. K. *Nano Letters* **2013**, *13*, 1555–1558.
- (8) Kim, M.-K.; Sim, H.; Yoon, S. J.; Gong, S.-H.; Ahn, C. W.; Cho, Y.-H.; Lee, Y.-H. *Nano Letters* **2015**, *15*, 4102–4107.
- (9) Laible, F.; Gollmer, D. A.; Dickreuter, S.; Kern, D. P.; Fleischer, M. *Nanoscale* **2018**, *10*, 14915–14922.
- (10) Muhammad, M.; Buswell, S. C.; Dew, S. K.; Stepanova, M. *Journal of Vacuum Science and Technology B, Nanotechnology and Microelectronics: Materials, Processing, Measurement, and Phenomena* **2011**, *29*, 06F304.
- (11) OpenCV Morphological Transformations Accessed: 25.08.2023, https://docs.opencv.org/4.x/d9/d61/tutorial_py_morphological_ops.html.
- (12) Rakic, A. D.; Djurisic, A. B.; Elazar, J. M.; Majewski, M. L. *Applied Optics* **1998**, *37*, 5271–5283.
- (13) PyGAD - Python Genetic Algorithm! — PyGAD 3.1.0 documentation, Accessed: [insert date here].
- (14) Zohar, N.; Chuntonov, L.; Haran, G. *Journal of Photochemistry and Photobiology C: Photochemistry Reviews* **2014**, *21*, 26–39.
- (15) Nordlander, P.; Oubre, C.; Prodan, E.; Li, K.; Stockman, M. I. *Nano Letters* **2004**, *4*, 899–903.
- (16) Prodan, E.; Radloff, C.; Halas, N. J.; Nordlander, P. *Science* **2003**, *302*, 419–422.
- (17) Savage, K. J.; Hawkeye, M. M.; Esteban, R.; Borisov, A. G.; Aizpurua, J.; Baumberg, J. J. *Nature* **2012**, *491*, 574–577.

A IMAGE MORPHING (PYTHON)

```
import numpy as np
import scipy as sp
import cv2

antenna_chromosome = "
011010100100110011000000100001010000000010001001001000110101001010000001001000
"
image_representation = np.array([int(i) for i in antenna_chromosome]).reshape(11,
11)

# upscale the image
upscaled_image = sp.ndimage.zoom(image_representation, 200, order=0)

# add padding zeros
upscaled_image = np.pad(
    upscaled_image, [(padding, padding), (padding, padding)], mode="constant")
# invert in order to make this cut extrude in COMOSL
inverted_image = np.logical_not(upscaled_image)

# make integer value for cv2
upscaled_image_uint8 = (inverted_image * 255).astype(np.uint8)

# calculate the kernel size to achieve the desired fillet radius
fillet_radius = 11 # radius in nm
image_size = np.size(
    upscaled_image_uint8[0])
) # number of pixels on one side of the image
substrate_size = 500 # nm, the sidelength of our simulation boundaries

pixel_per_nm = image_size / substrate_size
kernel_size = int(2 * fillet_radius * pixel_per_nm)

# create the structuring element
kernel = cv2.getStructuringElement(cv2.MORPH_ELLIPSE, (kernel_size, kernel_size))

# dilate and then erode the image
rounded_image = cv2.morphologyEx(upscaled_image_uint8, cv2.MORPH_OPEN, kernel)
rounded_image = cv2.morphologyEx(rounded_image, cv2.MORPH_CLOSE, kernel)

# save the image for visualization later
cv2.imwrite(image_path, rounded_image)
```

B GENETIC ALGORITHM PARAMETERS (PYTHON)

These are the parameters as determined via the simple summation heuristic fitness function. Shown as parameters of the PyGAD genetic algorithm initialisation function.

```
import pygad as pg

pg.GA(
    num_generations=400,
    num_parents_mating=15,
    fitness_func=fitness,
    sol_per_pop=40,
    num_genes=dim,
    init_range_low=0,
    init_range_high=2, #exclusive
    parent_selection_type="rank",
    keep_elitism=4,
    gene_type=int,
    crossover_type="uniform",
    mutation_percent_genes=4,
)
```